Development Of Prototype Simplified Neutron Scatter Camera for Nuclear Safeguards Applications

Taylor Harvey
University of Florida

Andreas Enqvist
University of Florida

ABSTRACT

Key in the international safeguards regime is the use of radiation detectors to track and characterize nuclear material. A relatively new area of interest in detector design is directional detectors: detectors that can report information on radiation source location and distribution. Neutron scatter cameras are a type of directional neutron detectors that rely on multiple neutron scatters to generate images that can reveal the direction and distribution of neutron sources. Fast neutron cameras which have recently been developed rely on multiple detector volumes and make use of neutron time-of-flight measurements. These designs, though effective in localizing the source direction, rely on a large amount of detection and electrical equipment, thus increasing the size, cost, and complexity of the systems to unreasonable levels for some applications. This project seeks to develop a compact scatter camera that is less expensive than systems relying on multiple detector volumes. Crucially, two components and capabilities are needed to achieve this: fast scintillation detection materials and picosecond electrical pulse timing. Utilizing such electronics, distinguishing between scintillation light pulses generated by the same neutron within one single detector volume is possible. A Monte Carlo model of such a system has been developed to guide prototype designs. A cube of EJ-230 fast plastic scintillator and six photomultiplier tubes (PMTs) were used to construct the prototype camera that localizes neutron sources based on the principle of cone back projection. Neutron scattering positions within the detector volume are found by comparing the timing and quantity of light arriving at PMTs mounted to opposing faces of the scintillator volume. The use of a digitizer with a sampling rate of 5 GHz allows for the identification of secondary scattering events. Prototypes of the system in one, two, and three dimensions have shown promising initial results when coupled with a script that algorithmically identifies candidate neutron double scatter events and back projects probability cones in the direction of possible sources. Imaging resolution, double scatter efficiency, and cost for the system is quantified. Paths forward for further improvement of a future system based on this camera's operating principles are discussed.

INTRODUCTION

The field of nuclear safeguards seeks to stop the spread of nuclear weapons by developing institutional, legal, and technical mechanisms intended to prevent the misuse of nuclear materials and technology [1,2]. Essential to the nuclear safeguards paradigm is the use of nuclear material measurement technologies to monitor and verify the quantity, identity, and movement of radioactive sources relevant to both peaceful and weapons programs. Of particular interest is Special Nuclear Material (SNM), such as uranium and plutonium, which can be monitored and identified using a variety of neutron detection techniques [3]. Much of the focus of nuclear material measurement technologies for safeguards is on destructive analysis (DA) and nondestructive assays (NDA) of nuclear material. Both DA and NDA techniques seek to determine properties of nuclear material through chemical, spectroscopic, or other means to make quantities known for material and accounting purposes. This suite of techniques can reveal,

often in fine detail, the "what" and "how much" of a material of interest but cannot give information about the location or distribution of a source if these facts are unknown. A new class of radiation detectors, known as directional or imaging detectors, seek to further the international safeguards technical repertoire by providing spatial information on radioactive sources.

Neutron scatter cameras (NSCs) operate by detecting two consecutive elastic scatters of a single fast neutron emitted by a nearby source. The kinematic principle involved in determining the original particle trajectory from two consecutive scattering events is similar to the operating principle of Compton cameras, though NSCs use fast neutrons rather than gamma rays [4]. The detector active volumes present in all currently existing NSCs use either organic liquid or plastic scintillators. The initial trajectory of individual neutrons is determined by finding the approximate (x, y, z) position of both the first and second scatter within the scintillator volume. The position of each scatter is found by either using spatially separated volumes of scintillators or by comparing the relative position and timing of the arrival of light to a series of photodetectors coupled to the same scintillator volume. Spatially separated arrays of scintillators may be arranged in either multiple planes or a radially symmetric arrangement. Mascarenhas *et al.* [5], Goldsmith *et al.* [6], and Weinfurther *et al.* [7] provide detailed technical discussions of the kinematics of scattering in plane-based, radial, and single-volume designs respectively. After the determination of two consecutive scatter positions and the determination of the energy deposited in the first scatter, probability cones encompassing the possible trajectories of individual neurons can be back-projected in 3-D space. The region of space where the surfaces of all the back projected cones overlap is interpreted to be the most likely direction of the neutron source.

Advances in both fast light pulse plastic scintillator materials and sub-nanosecond digitizer have allowed for the construction of compact or single-volume scatter cameras with high efficiencies and accurate angular imaging resolutions. Currently developed systems rely on photoelectronics and/or segmented designs that lead to systems with high unit costs and a high amount of data throughput from many digitized channels. The "simplified" prototype neutron scatter camera discussed in this paper proposes a design that is mobile, simple to use, and affordable while still providing useful data regarding the location, distribution, and identity of neutron-emitting sources.

DETECTOR DESIGN

An MCNPX-PoliMi model of a cube-shaped plastic scintillator volume was developed to guide the parameters of the simplified neutron scatter camera system. Simulation guided the selection of a 6'' side length cube of Eljen's EJ-230 fast plastic scintillator for the detection medium, six Electron Tube 9821KB photomultiplier tubes for the photodetectors, PSI's DRS4 digitizer for pulse digitization, and a custom MATLAB script for the data processing. These materials were selected to allow for the resolution of consecutive same-neutron scatters that appear only nanoseconds apart in time.

To create the back-projected probability cones needed to image neutron sources, the camera must be able to determine the scatter positions of neutron scatters one and two, the energy deposited in the first neutron scatter, and the time of flight between scatters one and two. In the simplified design, determination of the neutron scatter positions is done by comparing the amount

of light arriving at photomultiplier tubes coupled to opposing scintillator cube faces for voltage pulses algorithmically tagged as neutron double scatters. The double scatter pulse heights are proportional to the amount of light arriving at each PMT, which is itself proportional to the sighting factor from the scatter position to PMT photocathode, as described by the equation:

$$P_n = L_n log(NP_{n1}/NP_{n2}) \qquad (1)$$

Where P_n is the position along the n-dimension of the cube scintillator, L_n is the length of the scintillator in the n-dimension, and NP is the number of photons arriving at the two photodetectors oriented normal to the n-dimension. The scintillation position is localized in all three coordinates when this light intensity ratio comparison is done simultaneously across all six photodetectors. The energy deposited in the first neutron scatter is found by summing the light arriving at all six PMTs, determining the electron equivalent energy deposition corresponding to that amount of light, and calculating the proton recoil energy by using the electron equivalent value with the characteristic light curve for the scintillator material. The time of flight between the two neutron scatters is found by averaging the time between "peaks" corresponding to primary and secondary same neutron scatters in the pulse streams produced by each of the six PMTs. The relevant kinematic equations for cone back-projection are:

$$E_s = \frac{1}{2} m (\frac{d}{t})^2 \qquad (2)$$

$$E_i = E_f + E_s \qquad (3)$$

$$\theta_n = \sin^{-1} \sqrt{\frac{E_f}{E_i}} \qquad (4)$$

Where E_f is the energy deposited by the first neutron scatter, E_s is the neutron energy after the first scatter, E_i is the kinetic energy of a neutron from the source, m is the mass of the neutron, t is the time between scatters 1 and 2, d is the distance between scatter positions 1 and 2, and θ_n is the central angle of the back projected cone of possible source locations. Figure 1 summarizes the kinematics of double neutron scattering in the simplified design, and Figure 2 shows a photograph of the prototype simplified neutron scatter camera system.

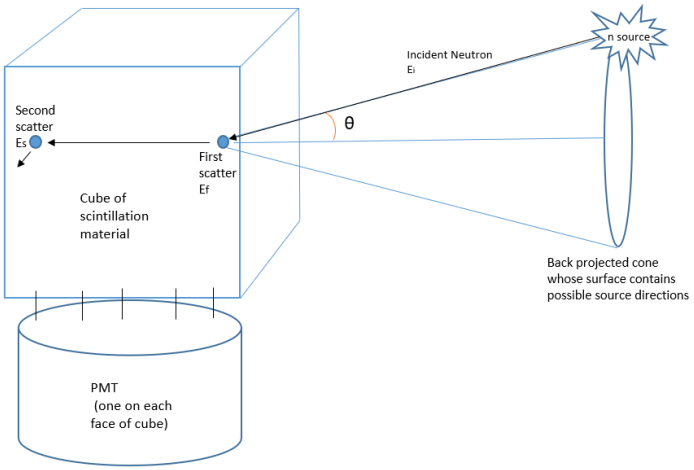

Fig. 1. Basic operating principle of a monolithic neutron scatter camera. Neutrons emitted by nearby sources must scatter at least twice in the scintillator volume. The scattering positions are determined by comparing the amount of

light arriving at each of the six PMTs mounted to the six surfaces of the scintillator. By solving a series of kinematic equations, a probability cone whose surface contains the possible trajectories of the neutron can be back-projected into 3-D space. Many correctly back-projected cones will converge to the source location.

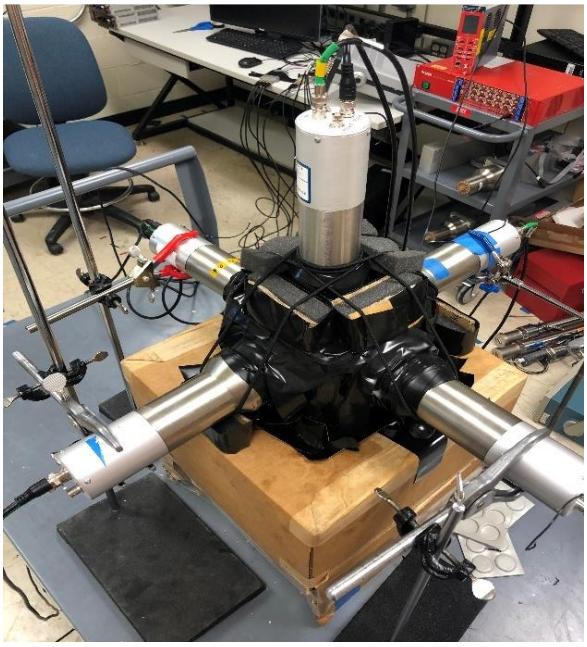

Fig. 2. Three-dimensional neutron scatter camera prototype. The PMT coupled to the bottom face is not visible as it is resting inside of the cardboard box support. Photo courtesy of the authors.

RESULTS

Point Source Measurements

A small 45 µCi ^{252}Cf spontaneous fission source was measured at a variety of angles relative to the camera to test the system's localization ability. Measurements of 5 million total counts at two different spatial positions resulted in the raw neutron images shown in Figure 3.

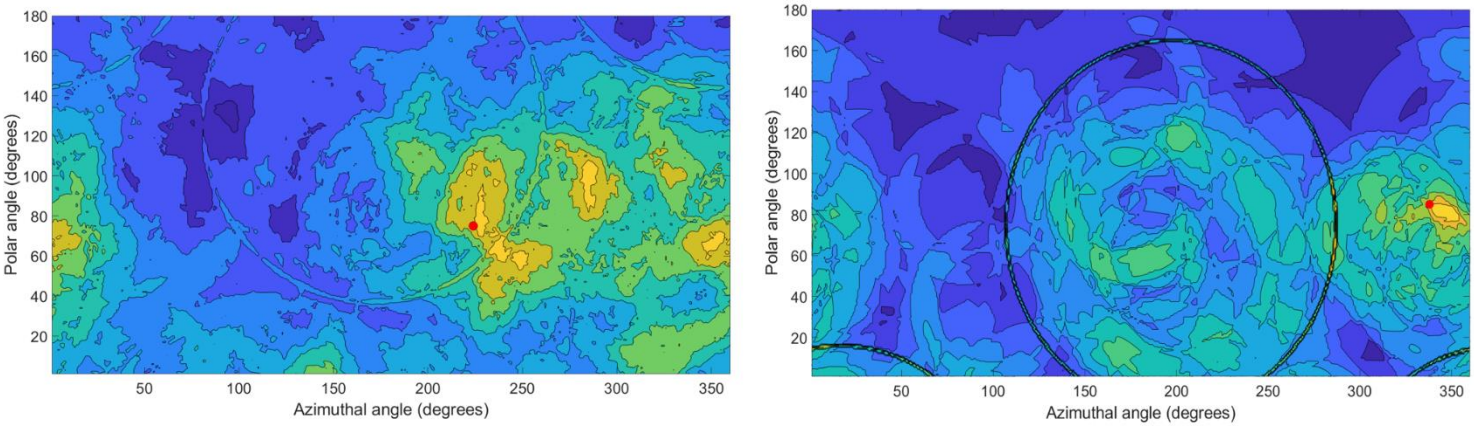

Fig. 3. Raw neutron images of point source measured at (224, 75) and (336,85). The left image was generated with a first scatter energy deposition cutoff of 0.2 MeV and a peak prominence ratio cutoff of 4. 154 cones were used to generate the image. The right image was generated with a first scatter energy deposition cutoff of 0 MeV and a peak prominence ratio cutoff of 2. 42 cones were used to generate the image.

Guess Vector Down-Selection

Observing the raw neutron images, it is clear that some of the probability cones do not overlap the neutron source region at all. Some of these erroneously positioned cones can be down-selected by first guessing at a general source direction and then eliminating any cones that do not have any part that intersects the guess region.

When analyzing the kinetic data used to make the raw neutron images, it was observed that the average interaction position for neutron first scatters within the scintillator cube was biased in the known direction of the point source. This insight suggests that the average interaction position for all scatters, not just the neutron double scatter used to create the probability cones, should be biased toward the direction of the source. This means that all voltage pulses detected by each of the six PMTs, and not just the neutron double scatters, can indicate a source direction by comparing the average skewness of log voltage pulse ratios between opposite PMTs with well-characterized reference values. To attain these reference values, a series of reference measurements were taken with neutron source 2 at various positions around the camera. First, two reference measurements were taken that should produce opposite PMT voltage pulse height ratio distributions with minimal skew: one with the neutron source positioned directly above the detector (along the positive z-axis) and the other positioned at the camera horizon level (in the x-y plane). The first of these reference measurements should minimize the scatter position-caused skew in the voltage pulse heights for the left/right and front/back PMT pairs, while the second does so for the top/bottom pair. Next, the bare neutron source was measured at a variety of positions along the azimuthal and polar axes of the camera system to generate three skew-source direction correlated curves. For each source position along the azimuthal and polar axes, adjusted skewness values can be found by subtracting the skew of the distribution of log light ratios at the measured position from the skew of the distribution of log light ratios at the reference positions (z-axis for left/right/front/back PMTS, x-y plane for top/bottom PMTs). These skew difference values can then be plotted along the known source positions in degrees to generate guess vector curves in the form:

$$guess\ vector_n = \alpha(PMT\_skew_n) + \beta \quad (5)$$

Where *guess vector* is the azimuthal or polar direction of the guess vector in degrees, *n* is the PMT pair, PMT_skew_n is the source position distribution skew for the nth PMT pair minus the appropriate reference value skew, and α and β are empirical constants used to convert between the skew difference value and source position degrees. Tables 1 and 2 display the data used to calculate the constants for these curves. The data points ranging from 0 to 180 azimuthal degrees were used for the left-right PMT curve, while the data points ranging from 90 to 270 azimuthal degrees were used for the back-front PMT curve.

Table 1. Neutron point source positions and corresponding adjusted log voltage ratio skew values.

Azimuthal source position (left-right/front-back) (°)	Left-right PMT adjusted skewness	Front-back PMT adjusted skewness	Polar source position (°)	Front-back PMT adjusted skewness
0/90	0.2637	0.2268	0	-0.0453
45/135	0.2124	0.2334	30	-0.0063
90/180	0.0709	0.2083	60	-0.0006
135/225	-0.1533	0.1232	90	0.1080
180/270	-0.1704	-0.0177	120	0.2051
225/315	-0.1147	-0.1499	150	0.2131

270/0	0.0900	-0.0958	180	0.3139
315/45	0.2529	-0.0638		

Table 2. Constants for source direction guess vector calculation using Equation 5-1.

PMT pair	α	β
Left-right (0 to 180 ° azimuthal)	-364.7	106.3
Front-back (90 to 270 ° azimuthal)	-510.7	187.0
Top-bottom (0 to 180 degree polar)	-488.0	145.0

The polar value determined from the skewness value of the voltage pulse heights in the top-bottom PMT pair ascertained from Equation 5 can directly be used in a guess vector for a source, though determining the azimuthal value requires an extra step. The distribution of voltage pulse ratios seen by either the left-right or front-back PMT pairs could result from either of two positions, calculated as the endpoint of the measured range (180° for left-right, 270° for front-back) plus-or-minus the adjusted skewness value. The two azimuthal source direction guesses produced through both the left-right PMT curve and the front-back PMT curve are compared to determine the most likely azimuthal source direction. The azimuthal component of the guess vector is selected to be the average degree value of the left-right/front-back guess paring that produces the smallest residual between the guesses. The source reference position calibration data needed to find the two components of the guess vector is imported into the MATLAB script along with the saved voltage pulse height ratio skews from all the coincident counts in the dataset to make the guess vector for improved images. The source direction guess vector can be used to improve images of neutron point sources by removing cones not overlapping the region around the guess vector. The removed cones result from erroneous kinetic calculations caused by multi-particle coincidence, room return neutrons, false positives caused by noise, or other errors that simulate the shapes of second scatter features in the correct time windows. The down-selection works by first creating the full contour plot of cone overlap for the original ‘raw’ image, plotting the location of the guess vector on that image, selected a region centered on the guess vector location and then removing all cones from the image that do not overlap in at least one degree bin with the guess vector region. A visual demonstration of this process is shown in Figure 4. The size of the guess vector region was varied and resulting images were analyzed for source point convergence and resolution. For neutron points sources, a quadrilateral guess vector region with a width of 60° azimuthal and a height of 20° polar was found to localize point sources with minimal noise.

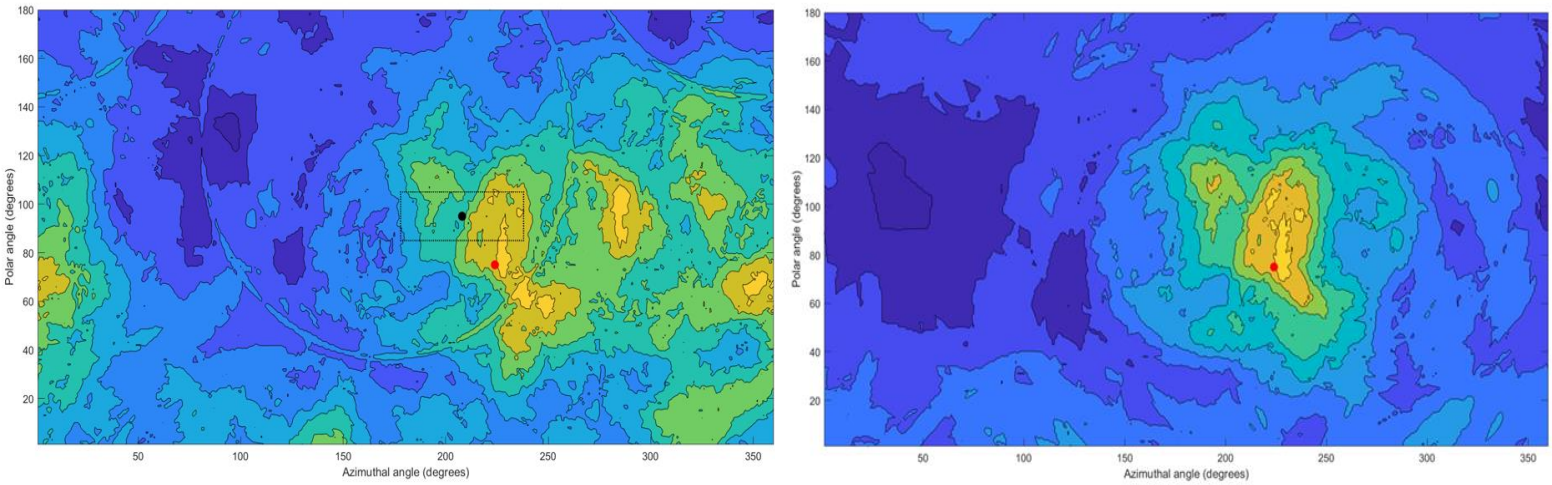

Figure 4. Demonstration of cone down-selection using source direction guess vector region. All cones that do not overlap the region outlined in black in the first image are removed to form the improved image.

In the datasets tested, the source direction initial guess vectors appeared anywhere from 3 to 45° from the true source direction. The guess vector region need not encompass the true source direction to improve the image, as is evident from Figure 4. Figure 5 shows more examples of improved neutron images along with the position of their guess vectors and true source positions. Using guess vector down-selection improves the images by removing erroneous cones that can lead to multiple hotspots with incorrect localization positions. Down-selection also improved the angular resolution of the true hotspots and, in cases with high numbers of probability cones, centers the hotspots on the true source position more consistently.

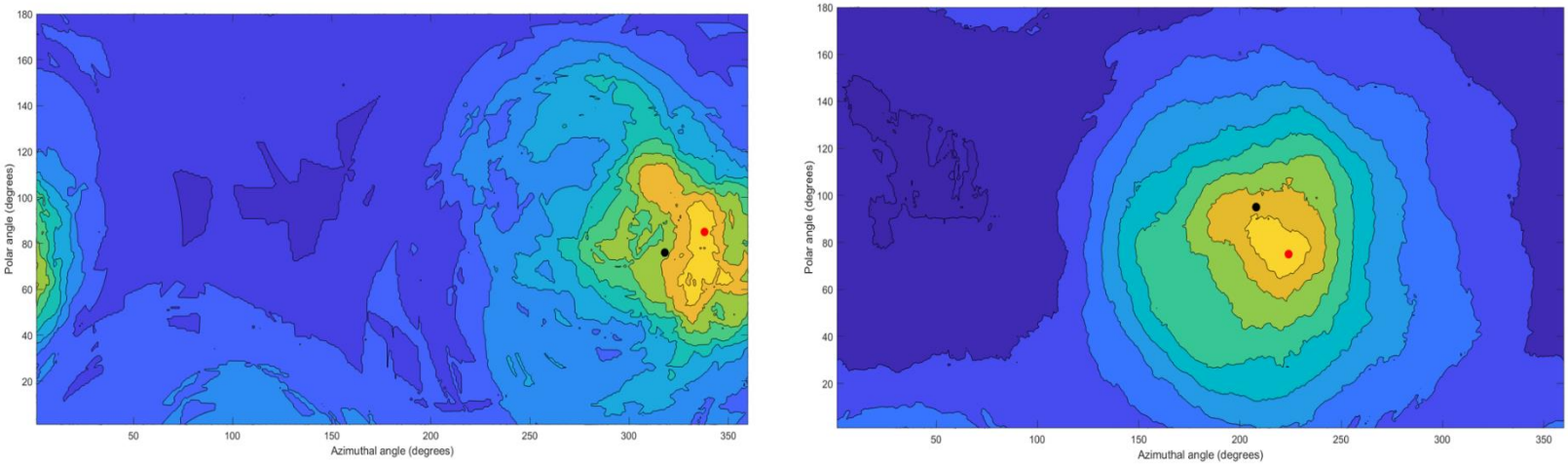

Figure 5. Improved neutron images of point sources located at (338, 85) and (224,75), with guess vectors pointing toward (318,76) and (208,95) respectively. The left image was made with an initial energy deposition cutoff of 0.5 MeV, a second scatter criterion prominence ratio of 6.5, and 48 cones. The right image was made with an initial energy deposition cut off of 0 MeV, a second scatter criterion prominence ratio of 4, and 654 cones. The guess vector regions were set to 60° azimuthal width and 20° polar height in both images.

Camera Performance

The imaging resolution of a camera-type radiation detector can be assessed through source position cross-cutting. The camera system does not have a single imaging resolution but rather a range of possible resolutions that vary with energy deposition cut offs, second scatter criterion, guess vector down-selection use, and guess vector down-selection region size. To assess this range of resolutions, the data from the point source measured at (18.3, 224, 75) was iteratively run through the neutron image creation portion of the script while varying both the energy deposition cutoff and the second scatter criterion. A series of images corresponding to each cutoff value was saved for both the raw images and improved images (those that used guess vector down-selection). The resolution of each image was then determined by crosscutting each of the images in the polar and azimuthal directions at the known source location. In many cases, the peak of these crosscuts did not correspond to the true source direction. In these cases, the azimuthal and polar error between the true source position and the images' maximum probability pixel weight value are

recorded. Table 4 lists the resolution values, localization errors, and the number of probability cones for a range of improved neutron images. In cases where multiple probability hotspots appeared along a crosscut, the peak corresponding to the hotspot nearest to the true source position was used for resolution and error determination. Images were determined to have "no convergence" if a hotspot of at least 80% of the probability of the hottest projection bin was not within 60 degrees of the true source position.

Table 3. Resolutions of improved neutron images over a range of algorithm parameters. The data in each cell is reported in the form: (azimuthal resolution, azimuthal error, polar resolution, polar error, number of cones). The resolutions and errors are reported in degrees.

	First scatter energy deposition cutoff (MeV)			
Peak prominence ratio cutoff	0	0.2	0.4	0.6
5	(44,1,38,9,413)	(49,16,41,4,183)	(54,33,41,17,55)	(30,30,20,13,16)
4.5	(42,13,40,5,289)	(39,20,39,11,116)	(56,18,29,14,33)	(38,9,26,13,12)
4	(31,20,43,15,176)	(43,16,29,3,87)	(44,23,29,17,25)	No convergence
3.5	(31,1,31,3,104)	(30,22,24,3,42)	No convergence	No convergence
3	(43,23,34,10,67)	(40,23,31,16,30)	(31,8,25,7,9)	No convergence
2.5	(54,22,37,6,35)	(37,19,23,17,17)	No convergence	No convergence
2	(30,3,45,2,23)	No convergence	No convergence	No convergence
1.5	(20,3,23,10,13)	No convergence	No convergence	No convergence

Like the resolution determination, the camera system will not have a single double scatter efficiency but rather a range of achievable efficiencies determined by the cutoff values used in the determination of which pulse sestets are used in cone generation. To test the camera system's useful cone efficiency, a measurement of 12 million counts generated from the two ^{252}Cf point sources together was run iteratively over a range of cutoffs. The sources were position together and shielded with three lead bricks to simulate a "pure" neutron source free from non-background gamma rays. The datafile was iteratively run through section 2 of the double pulse identification algorithm, with either the peak prominence ratio cutoff or the first scatter energy deposition cutoff changed at each step. At each iteration, the useful cone efficiency for those settings was determined by dividing the double scatter candidate identified by the total counts in the data file. Figure 6 shows a series of useful cone efficiency curves at different cutoff values. As the first scatter energy deposition cutoff value is increased, the useful cone efficency decreases in a log-linear fashion across the range of peak prominence ratio cutoffs. These curves can be used to guide the selection of cutoff values for the desired count rate or measurement time as needed.

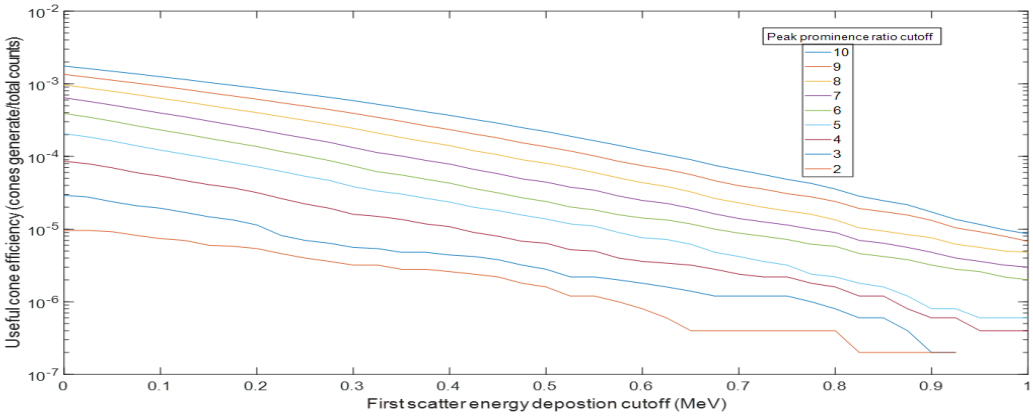

Fig. 8. Useful cone efficiency curves for the camera system prototype.

System Economics

The simplified NSC concept is not intended to have the best possible angular resolution nor optimal imaging efficiency, but rather is intended to provide adequate neutron source localization abilities in a wide variety of measurement scenarios by being both physically transportable and relatively inexpensive. The largest expenses for an NSC system are made up of the scintillator materials, the photomultipliers, and the digitization electronics. Table 5 summarizes the cost of the simplified NSC by breaking down the approximate cost of each component of the camera in July 2021 dollars. The cost breakdown excludes the cost of a computer and data processing software.

Table 5. Breakdown of cost of Simplified Neutron Scatter Camera prototype.

Component(s)	Approximate cost ($)
6'' EJ-230 scintillator cube	1900
Six Electron Tube 9821KB photomultiplier tubes	9000
Two PSI DRS4 four-channel digitizers	4000
Six-channel variable high voltage power supply	1500
Light-proofing tape, optical greasing, and cables	200
Total cost	16600

The figure of $16600 per unit is considerably less expensive than existing NSC systems due to the reduced number of scintillator volumes, photomultipliers, and fully digitized channels used. Systems with high numbers of these components can run from multiple tens of thousands to millions of dollars per unit. Systems with high cost and complexity generally make them undesirable for deployment in many safeguards scenarios.

CONCLUSIONS

The NSC presented in this paper is but one among many designs that have been developed or are in development with the end goal of strengthening global nuclear security through neutron source imaging, localization, and spectroscopy. No one NSC system proposed can satisfy the needs presented by all nuclear safeguards scenarios, which require a range of imaging resolutions, efficiencies, spectroscopic abilities, portability levels, data channel numbers, and costs. The safeguards community currently has multiple design approaches for NSCs, meaning that policymakers and engineers may choose from a variety of complimentary designs for different goals as needed.

The Simplified Neutron Scatter Camera presented here is not the optimum choice among the competing design for superior imaging resolution or efficiency. In its current non-rugged form, it is also not quite portable, though it could be made so with some minor changes. The strengths of the simplified NSC lay in its ability to localize neutron sources with a low number of digitized channels and a low unit cost when compared to other systems. These facts could make an optimized system using similar methods and materials attractive to produce for safeguards settings in batches.

The initial Simplified NSC system also provided an early-stage proof-of-concept for the ability to resolve and localize consecutive single-neutron scatters only nanoseconds apart in time in a single fast plastic scintillator outfitted with standard PMTs and sub-nanosecond digitizers. The algorithm to identify such events and the guess vector down-selection method to eliminate false positives are likely the most valuable findings emerging from this research project. With further refinement of the double scatter identification algorithm, optimizing of the detector

volume and photomultiplier size, explorations of different scintillator materials, reflectors, and photomultipliers, and the honing of the imaging down-selection method, a detector using the Simplified Neutron Scatter Camera design could become a valuable tool for international nuclear safeguards.

ACKNOWLEDGMENTS

The authors would like to acknowledge the Consortium for Monitoring, Technology, and Verification (MTV) for partially funding this research.

REFERENCES

[1] International Atomic Energy Agency. "Basics of IAEA Safeguards," [Online] Available: https://www.iaea.org/topics/basics-of-iaea-safeguards. Accessed on" June 30, 2021.

[2] J.E. Doyle. "Introduction: Nuclear Security and Global Challenges," in *Nuclear Safeguards, Security, and Nonproliferation*, 1st ed. Burlington, MA, USA: Butterworth-Heinmann, 2008.

[3] R.C. Runkle, A. Bernstein, and P.E. Vanier, "Securing Special Nuclear Material: Recent Advances in Neutron Detection and Their Role in Nonproliferation," Journal of Applied Physics, vol. 108, no. 11, 2010, 10.1063/1.3503495.

[4] D. Xu, Z. He, C.E. Lehner, F. Zhang. (2004, August). 4-pi Compton Imaging with Single 3D Position Sensitive CdZnTe Detector. Presented at SPIE 5540, Hard X-Ray and Gamma-Ray Detector Physics VI. [Online]. Available: doi.org/10.1117/12.563905. Accessed on: June 30, 2021.

[5] N. Mascarenhas, J. S. Brennan, and K. Krenz. (2006, October). Development of a Neutron Scatter Camera for Fission Neutrons. Presented at: 2006 IEEE Nuclear Science Symposium. [Online]. Available: https://www.semanticscholar.org/paper/Development-of-a-Neutron-Scatter-Camera-for-Fission-Mascarenhas-Brennan/a3544f4fbce0f4c048d11c2577ad2ab3d0ddb0e7. Accessed on: June 30, 2021.

[6] J. E. M. Goldsmith, M.D. Gerling, J.S. Brennan, "A compact neutron scatter camera for field deployment," Review of Scientific Instruments, Vol. 87, August 2016, DOI. 10.1063/1.4961111.

[7] K. Weinfurther, J. Mattingly, E. Brubaker, J. Steele, "Model-Based Design Evaluation of a Compact, High-Efficiency Neutron Scatter Camera," Nuclear Instruments and Methods in Physics Research Section A, Vol. 883, pp. 115-135. March 2018. DOI. 10.1016/j.nima.2017.11.025.

[8] J.J. Manfredi, B.L. Goldblum, T.A. Laplace, G. Gabella, J. Gordon, A. O'Brien, S. Chowdhury, J.A. Brown, and E. Brubaker, "Proton Light Yield of Fast Plastic Scintillators for Neutron Imaging," IEEE Transactions in Nuclear Science, vol. 67, no. 2, pp. 434-442, December 2019. DOI. 10.1109/TNS.2019.2959979.